Paraelectric-ferroelectric phase transitions of KH_2PO_4, RbH_2PO_4, and KH_2AsO_4 studied by infrared reflectivity

Patrick Simon and François Gervais
Centre de Recherche sur la Physique des Hautes Températures, Centre National de la Recherche Scientifique, 45071 Orléans Cedex 2, France

Eric Courtens
IBM Research Division, Zurich Research Laboratory, Saümerstrasse 4, 8803 Rüschlikon, Switzerland
(Received 9 March 1987)

The infrared-reflectivity spectra of KH_2PO_4 (KDP) and its isomorphs RbH_2PO_4 (RDP) and KH_2AsO_4 (KDA) are reported in a wide spectral range (from 20 to 4000 cm^{-1}), in the paraelectric and ferroelectric phases. The phonon responses are obtained by fitting the factorized form of the dielectric function to the experimental spectra. The comparison of the data obtained in the three compounds allows the assignment of all vibrational modes. In RDP, the internal ν_{4c} polar mode polarized along the ferroelectric axis is found to soften upon approaching T_C from below or above, although to a lesser extent. The eigenvector pattern of this mode shows that it interacts strongly via electrostatic coupling with the intersite tunneling proton motions perpendicular to the ferroelectric axis. This phenomenon is thought to be the origin of the ν_{4c} mode softening. This mode also couples with other polar modes of the same symmetry via a mechanism intermediate between Fano-type interference and classical mode-mode coupling. The coupled excitation evolves to yield the overdamped ferroelectric mode that triggers the paraelectric-ferroelectric phase transition. The temperature dependence of its oscillator strength agrees with that of the dielectric constant measured above piezoelectric resonances or in single domain samples. The temperature dependence of the effective charges carried by the ions, deduced from TO-LO splittings, is also consistent with a displacive mechanism.

I. INTRODUCTION

Potassium dihydrogen phosphate and its isomorphs [RbH_2PO_4 (RDP), KH_2AsO_4 (KDA), KD_2PO_4 (DKDP),...] undergo a paraelectric ($I\bar{4}2d$) to ferroelectric ($Fdd2$) phase transition, which was evidenced more than fifty years ago by Busch and Scherrer.[1] Nowadays, we know unambiguously from recent high-resolution neutron-diffraction measurements[2,3] that the protons or deuterons are disordered between two positions in the paraelectric phase, along the O—H—O bonds. It is generally considered that deuteron motions between these positions are essentially relaxational, while protons can cross the potential barrier from one well to the other by tunneling effect. This concept of proton tunneling was introduced by Blinc[4] to explain the large increase of Curie temperatures upon deuteration. Tunneling induces a proton collective mode,[5] the coupling of which with the lattice modes may explain the appearance of a spontaneous polarization perpendicular to the proton motions. Kobayashi[6] has shown that the interaction of the proton collective mode with the K^+-PO_4^{3-} translational vibration mode of B_2 symmetry (polarization parallel to the ferroelectric axis) yields two coupled modes, denoted ω_+ and ω_-, the latter exhibiting a soft-mode behavior. This soft mode was previously observed in the low-frequency infrared reflectivity spectra of Barker and Tinkham,[7] and later in the Raman-scattering experiments of Kaminow and Damen.[8] It is overdamped at any temperature, but under high hydrostatic pressure (above 6 kbar), it becomes slightly underdamped, with a frequency-to-damping ratio equal to 1.18 at 9.3 kbar, as shown by the Raman-scattering measurements of Peercy.[9] All these theoretical and experimental investigations were recently reviewed,[10–14] and the phase transition appears connected with the condensation of a soft mode, which comes from the interaction of the proton collective mode with the translational optical mode K^+-PO_4^{3-}, and also with the X_y shear acoustic mode, the interaction of which with both others being a piezoelectric coupling.[15]

Recently, a new interpretation[13,16] based upon the observation above T_C of Raman lines, symmetry forbidden in the paraelectric phase but allowed in the ferroelectric phase, in KDP,[17–19] DKDP,[20] RDP, and RbD_2PO_4 (DRDP) (Ref. 21) has been proposed. According to which, the phase transition would be due to an order-disorder behavior of the whole rigid cluster H_2PO_4, without proton tunneling, and without soft mode. The low-frequency response would then be a relaxational excitation instead of the overdamped soft mode generally considered.

Infrared-reflectivity spectroscopy associated with the simulation of the experimental spectra by a dielectric function model, such as the factorized form,[22] is a powerful method to investigate a ferroelectric soft-mode behavior, and may help to clarify the problem related to this controversy. This spectroscopy provides the struc-

ture of the polar modes, the intensities of which are nothing but their dielectric strength. Earlier infrared-reflectivity studies were limited to narrow frequency ranges. Most experimental spectra were analyzed by Kramers-Kronig inversion.[7,23–25] Owing to the weakness of the classical Born-Huang dielectric function, found inappropriate to fit such spectra, the Barker-Hopfield coupled-mode model[26] has been applied to fit both lowest-frequency modes.[27,28] Simulations of infrared-reflectivity spectra with the factorized form of the dielectric function were reported just recently,[29,30] but they were carried out only in the low-frequency range (below 400 cm^{-1}), and for KDP alone.

The aim of this paper is to report and compare the whole (20–4000 cm^{-1}) infrared-reflectivity spectra of three KDP-type compounds (KDP, $T_C=123$ K; RDP, $T_C=145$ K; KDA, $T_C=96$ K), above and below T_C, for the electric field of the infrared radiation polarized parallel or perpendicular to the ferroelectric axis. A fit of the factorized form of the dielectric function to reflectivity data yields the structure of the polar modes, whose comparison in the three compounds allows their assignments.

II. EXPERIMENTAL PROCEDURE

The infrared-reflectivity spectra have been recorded with a Bruker IFS 113C rapid-scan Fourier-transform interferometer, giving access to the spectral range 20–4000 cm^{-1} (for a more complete description, see Ref. 22). Low temperatures were obtained by using a liquid-nitrogen cryostat, with polyethylene (far-infrared) and KRS-5 (thallium bromoiodide, near-infrared) windows. The temperature stability is better than 1 K. The samples were cut into plates about 1 cm×1 cm×1 mm in size, the ferroelectric axis lying within the largest face of the plate.

III. ANALYSIS OF INFRARED-REFLECTIVITY SPECTRA

A. Dielectric function models

Theoretically, the real and imaginary parts of the dielectric function $\epsilon(\omega)$ can be deduced from the reflectivity spectrum $R(\omega)$ by Kramers-Kronig inversion. In practice, it appears that the errors involved in calculating the phase from the reflectivity lead to a dielectric function often less accurate than the result of a fit of an appropriate dielectric function model to the experimental spectra. The usual method is to use the classical dielectric function

$$\epsilon(\omega)=\epsilon_\infty+\sum_j \Delta\epsilon_j \frac{\Omega_{j\mathrm{TO}}^2}{\Omega_{j\mathrm{TO}}^2-\omega^2+i\gamma_{j\mathrm{TO}}\omega} . \tag{1}$$

Equation (1) will be referred to as the three-parameter model, or sum formula of the dielectric function. Each polar mode is described by three adjustable parameters, frequency $\omega_{j\mathrm{TO}}$, damping $\gamma_{j\mathrm{TO}}$, and dielectric strength $\Delta\epsilon_j$. This model fits the experimental spectra of numerous compounds satisfactorily, except when the spectra exhibit wide reflection bands, i.e., large TO-LO splittings. This discrepancy is due to implicitly then assuming the same phonon decay for two phonon energy levels far apart. To improve this, one may use the factorized form of the dielectric function, or four-parameter model[31]

$$\epsilon(\omega)=\epsilon_\infty\prod_j \frac{\Omega_{j\mathrm{LO}}^2-\omega^2+i\gamma_{j\mathrm{LO}}\omega}{\Omega_{j\mathrm{TO}}^2-\omega^2+i\gamma_{j\mathrm{TO}}\omega} . \tag{2}$$

Note that when $\omega=0$, Eq. (2) is nothing but the Lyddane-Sachs-Teller relation; ϵ is obtained by factorizing over poles and zeroes (the transverse and longitudinal optical modes, respectively). Each TO or LO mode is described by two parameters, frequency and damping, the oscillator strength of mode j then being obtained from all TO and LO frequencies

$$\Delta\epsilon_j=\frac{\epsilon_\infty}{\Omega_{j\mathrm{TO}}^2}\frac{\prod_k(\Omega_{k\mathrm{LO}}^2-\Omega_{j\mathrm{TO}}^2)}{\prod_{k\neq j}(\Omega_{k\mathrm{TO}}^2-\Omega_{j\mathrm{TO}}^2)} . \tag{3}$$

This model has been shown to describe numerous spectra satisfactorily, even in the case of relaxational excitations.[22]

B. Symmetry of the vibration modes

In both paraelectric and ferroelectric phases, KDP-type crystals contain two formula units per primitive

TABLE I. Reduction into irreducible representations of the 45 normal optical modes of KDP-type compounds in the paraelectric phase ($I\bar{4}2d$) for $T>T_C$. g denotes the degeneracy of the representation; N_{tot} the total number of modes, N_{T}, N_{L}, and N_{H} the number of translational external, librational, and proton modes, respectively. The number of tetrahedron internal modes is indicated with Herzberg's notations (after Refs. 13 and 32).

	g	N_{tot}	N_{T}	N_{L}	N_{H}	Internal modes	Basis function Raman and ir activities
A_1	1	4	0	1	1	$\nu_1+\nu_2$	$xx+yy,zz$
A_2	1	5	0	1	2	$\nu_1+\nu_2$	
B_2	1	6	1	0	2	$\nu_2+\nu_3+\nu_4$	xy,P_z
B_1	1	6	2	0	1	$\nu_2+\nu_3+\nu_4$	$xx-yy$
E	2	12	3	2	3	$2\nu_3+2\nu_4$	$\begin{cases} yz,P_x \\ xz,P_y \end{cases}$

TABLE II. Reduction into irreducible representations of the 45 normal optical modes of KDP-type compounds in the ferroelectric phase (*Fdd*2). For the notations, see Table I. For $T < T_C$, $x' = \frac{1}{2}(x+y)$ and $y' = \frac{1}{2}(x-y)$ (after Refs. 13 and 32).

	g	N_{tot}	N_T	N_L	N_H	Internal modes	Basis function Raman and ir activities
A_1	1	10	1	1	3	$\nu_1+2\nu_2+\nu_3+\nu_4$	$x'x', y'y', zz, P_z$
A_2	1	11	2	1	3	$\nu_1+2\nu_2+\nu_3+\nu_4$	$x'y'$
B_1	1	12	3	2	3	$2\nu_3+2\nu_4$	$x'z, P_{y'}$
B_2	1	12	3	2	3	$2\nu_3+2\nu_4$	$y'z, P_{x'}$

cell, i.e., 16 atoms. Tables I (paraelectric phase) and II (ferroelectric phase) show how the 45 normal optical modes transform as the irreducible representations of the space groups. This classification assumes local symmetry S_4 for the tetrahedron, viz., averaged symmetric O—H—O bonds. The ferroelectric axis is the z axis with the notations of Tables I and II, and the soft mode is of B_2 symmetry above T_C and A_1 below. Modes of these representations are infrared active, for a polarization of the infrared electric field along the ferroelectric axis. The E modes of the paraelectric phase are infrared active for the electric field polarized in the plane perpendicular to the ferroelectric axis, and split into B_1 and B_2 modes below T_C, owing to the loss of the fourfold axis. There is no inversion center in either phase, so each infrared active mode is also Raman active.

IV. RESULTS AND DISCUSSION

The infrared-reflectivity spectra were recorded from liquid nitrogen up to room temperature, and for both polarizations of the electric field: parallel to the ferroelectric c axis (B_2 symmetry above T_C, A_1 below), or perpendicular to it. The a and b twofold axes of the high-temperature phase (E symmetry) are rotated by 45° from the a or b axis of the low-temperature phase (B_1+B_2 symmetry). No precaution was taken to ensure monodomain samples, since (i) domains of opposite directions give the same infrared spectrum polarized along the ferroelectric axis; (ii) dynamic effects owing to domains are expected only at frequencies below the infrared range. For the perpendicular polarization, the former argument is no longer valid, and one must consider the whole spectrum as a combination B_1+B_2.

The infrared reflectivity spectra of KDP-type compounds are really unusual, with all reflection bands displaying anomalously asymmetric profiles more or less pronounced, some of them being characteristic of highly damped excitations (Figs. 1 and 2).

A. *E* parallel to the ferroelectric axis

Typical spectra are shown in Figs. 1 and 2. The imaginary dielectric function (i.e., the TO-mode response) was first obtained from the experimental spectra by Kramers-Kronig inversion, the result of that analysis then forming the starting point for simulation of the spectra with the factorized form of the dielectric function. Figure 1 illustrates the effect of the fourth adjustable parameter: the experimental spectrum of RDP at 295 K is plotted with the best fit with the factorized

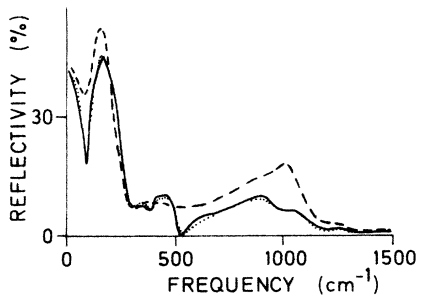

FIG. 1. Infrared-reflectivity spectrum (full line) of RDP ($T=295$ K) polarized along the ferroelectric axis. Dotted line: best simulation obtained with the four-parameter model of the dielectric function. Dashed line: result of the three-parameter model fit obtained by taking same TO frequencies, dampings, and oscillator strengths as in the four-parameter plot.

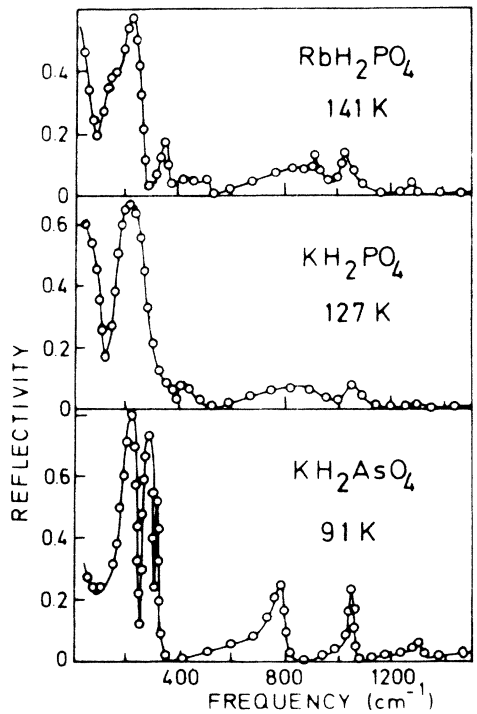

FIG. 2. Experimental infrared-reflectivity spectra (open circles) and best simulations obtained with the four-parameter model of the dielectric function (full line) for RDP, KDP, and KDA for the electric field of the electromagnetic wave polarized along the ferroelectric axis.

form of the dielectric function. The dashed line is calculated with the three-parameter model assuming the same TO frequencies, TO dampings and oscillator strengths as in the four-parameter plot. The discrepancy between the dashed and dotted curves illustrates the effect of phonon-line asymmetries that obviously cannot be described by a single damping parameter. The quality of the fit with the factorized form shows that the description of damping profiles with only two parameters is sufficient. This is particularly striking in KDP-type compounds owing to strong asymmetries of the lines due to Fano-type interferences[33,34] between discrete and highly damped modes. This illustrates once again the power of the four-parameter model.[22] Figure 2 shows one typical example of such a simulation per compound. Complete numerical results are available elsewhere.[35]

The TO-mode structure is plotted in Fig. 3 for the three compounds and at two temperatures in each case. Apart from the very low frequency region (below 100 cm^{-1}), the spectra are practically temperature independent in the paraelectric phase. According to Table I, comparison of the compounds allows identification of the lattice modes above T_C: the cation (Rb^+ or K^+)–anion ($H_2PO_4^-$ or $H_2AsO_4^-$) translational mode lies just below 200 cm^{-1}; the two proton modes are at the same frequencies in the three compounds, at about 1035 and 1300 cm^{-1} (the O—H bonds are the only ones unchanged in all compounds), and the three internal modes allowed appear at the same frequencies in both phosphates, and at lower frequencies in the arsenate, consistent with the natural frequencies of the molecular ions.[36] Upon cooling below the Curie temperature, additional modes appear according to symmetry predictions (Table II). The librational mode lies near 120 cm^{-1} in RDP at 80 K, is not observed in the other compounds, but is visible below 60 K in KDP.[37] Two additional internal modes are also observed according to symmetry predictions.

In the high-temperature phase, all the modes observed experimentally are symmetry allowed, apart from the lowest-frequency overdamped mode. Figure 3 also shows that the imaginary dielectric function vanishes between 500 and 700 cm^{-1}, which means that high-frequency modes (ν_3, ν_1, and bending O—H modes) are decoupled from low-frequency ones. This is even more pronounced in RDP. Hence, a discussion of the overdamped mode may be limited to the range 0–500 cm^{-1}, at least for this polarization.

Figure 4 displays the temperature dependence of the imaginary dielectric function of RDP. Below 600 cm^{-1}, at the lowest temperatures (80 K), all modes except the internal ν_{4c} mode are only slightly damped. Damping of the ν_{4c} mode, although subcritical, is surprisingly high even at 80 K. The overdamped mode has vanished at this temperature. It appears only upon heating above about 100 K. The low-frequency mode parameters (TO and LO frequencies, and oscillator strengths) are plotted in Fig. 5. Upon approaching T_C from below, the ν_{4c} mode frequency decreases, while its oscillator strength increases strongly and is multiplied by five between 80 K and T_C. Both these phenomena are characteristic of mode softening. The ν_{4c} mode pushes down the translational external mode with an increase of its oscillator

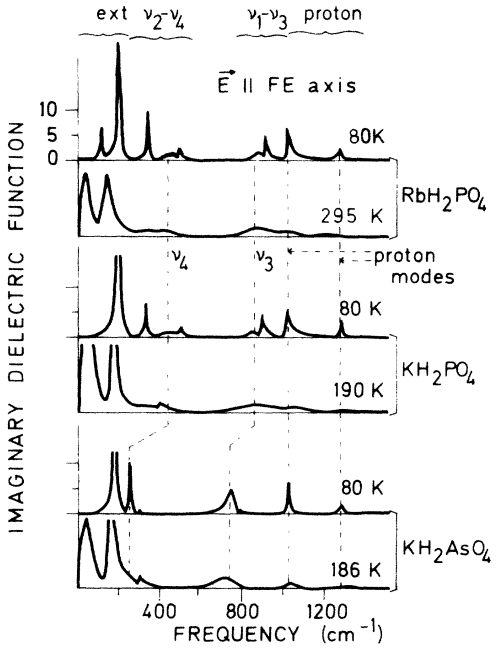

FIG. 3. Imaginary dielectric function (structure of TO modes) deduced from the simulation of the experimental spectra with the four-parameter model for RDP, KDP, and KDA (polarization along the ferroelectric axis).

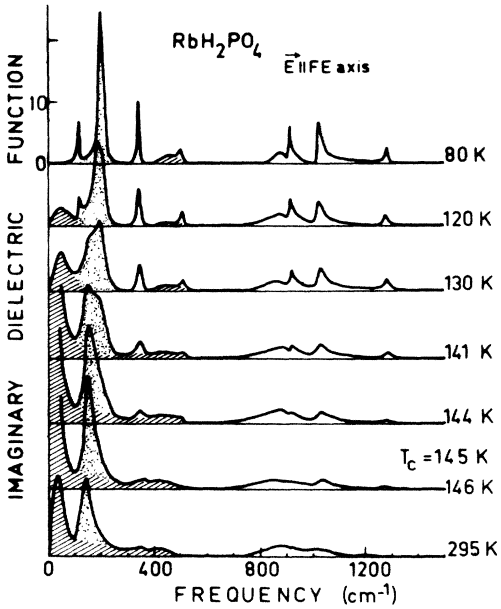

FIG. 4. Temperature dependence of the structure of the TO modes for RDP (polarization along the ferroelectric axis). The Rb-H_2PO_4 translational mode is dotted, while the hatched regions correspond to the overdamped soft mode and to the ν_{4c} mode.

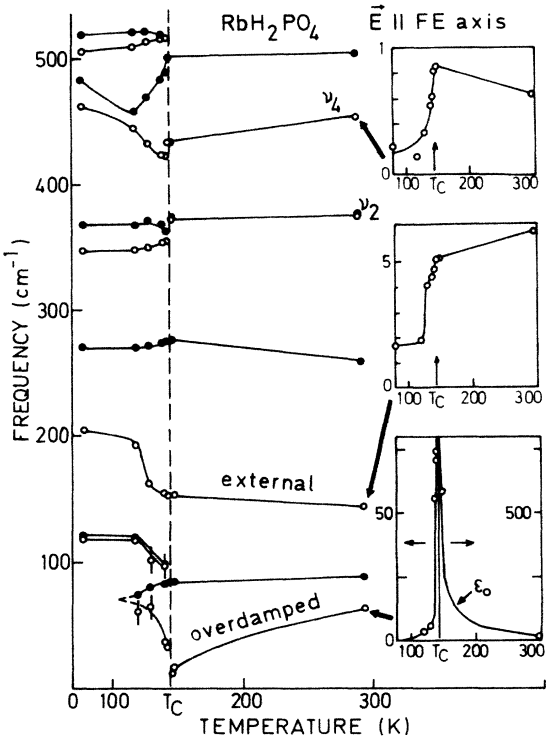

FIG. 5. Temperature dependence of the LO (full circles) and TO (open circles) lowest-frequency mode frequencies of RDP (polarization along the ferroelectric axis). Inserts show the temperature dependence of the oscillator strength of the modes denoted by the arrows. The lines are guides to the eye.

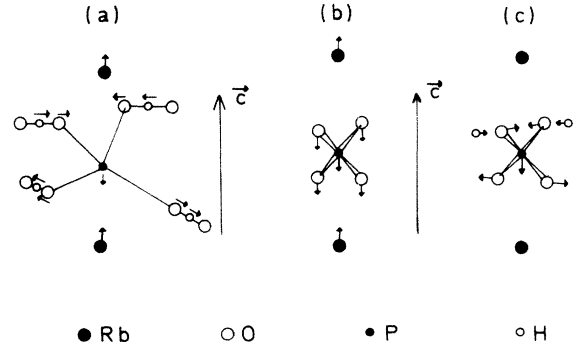

FIG. 6. Representation of (a) the overdamped soft-mode eigenvectors, i.e., static displacements of the ions at the phase transition; (b) the low-frequency Rb-H_2PO_4 translational external mode eigenvectors; and (c) the ν_{4c} eigenvectors.

strength; the larger the strength, the stronger this anticrossing effect. Therefore, the weak ν_2 mode, between the ν_{4c} and the external modes, is not significantly affected by the ν_{4c} softening. Near T_C, the external mode slowing down saturates, and the overdamped mode then appears below 100 cm^{-1}. This is the ferroelectric soft mode, labeled ω_- by Kobayashi.[6] At T_C, its frequency is minimum and its oscillator strength maximum, but also—the most important point—its oscillator strength amounts to the dielectric constant or nearly so, at least when measured in the millimetric range,[38] or on a single-domain sample[39] to avoid contributions from domain structure motions. This lowest frequency mode dominates the dielectric response in the vicinity of T_C to such a degree that its oscillator strength is almost two orders of magnitude larger than that of all other modes. This enormous component is described here by an overdamped mode; its propagative character was demonstrated by Peercy's Raman experiments under pressure.[9]

The eigenvectors of the ω_- ferroelectric soft mode, of the external mode and of the ν_{4c} mode are drawn in Fig. 6. Obviously, the intersite proton motion couples strongly to the ν_{4c} mode, by electrostatic interaction; it is not infrared active in this polarization, but its interaction with the ν_{4c} mode is thought to explain the strong damping of the latter. These facts lead us to propose the following interpretation: upon approaching the phase transition from below, the onset of intersite proton motions destabilizes the internal ν_{4c} mode which softens. It couples with lower-frequency modes, particularly with the most polar one, i.e., the Rb-PO_4 translational mode. The ν_{4c} mode partially transfers its eigenvectors to this external mode, yielding the ω_+ mode in Kobayashi's description. Mode ν_{4c} remains blocked above the LO mode immediately lower (ν_2), according to the anticrossing rule of discrete states.

Upon approaching T_C, the proton disorder increases, resulting in an ever wider spectral response for the ν_{4c} mode: the coupled excitation (H,ν_{4c}, external mode) evolves into a quasicontinuum. Then the coupling between this broad excitation and discrete states is better described by Fano-type interaction[33,34] than by the classical mode-mode coupling, consistent with the asymmetric line shapes of the phonon responses (see, for instance, the ν_2 modes). In the case of Fano-type interaction, a continuum may cross a discrete state. This explains the appearance of the quasicontinuum (H,ν_{4c}, external mode) at low frequencies, which is nothing but ω_- Kobayashi's mode, and described here by an overdamped mode.

Summarizing, the ferroelectric soft mode is the low-frequency overdamped mode, but the random intersite proton motions perpendicular to the ferroelectric axis, which are at the origin of the phase transition, affect the ν_{4c} mode first. Since these proton motions are not taken into account by group theory, this additional degree of freedom gives rise to an additional mode via coupling with the normal modes with which it interacts preferentially.

The situation is presumably the same in other compounds. In KDP (Fig. 7), the ν_{4c} and the main external modes shift down at the same temperature within experimental error, while the overdamped mode appears at low frequency. The oscillator strength of this mode corresponds to the dielectric constant value,[39–41] near or above T_C. The experimental signature of the phenomenon however is less visible than in RDP for two reasons. (i) The phase transition is of first order in po-

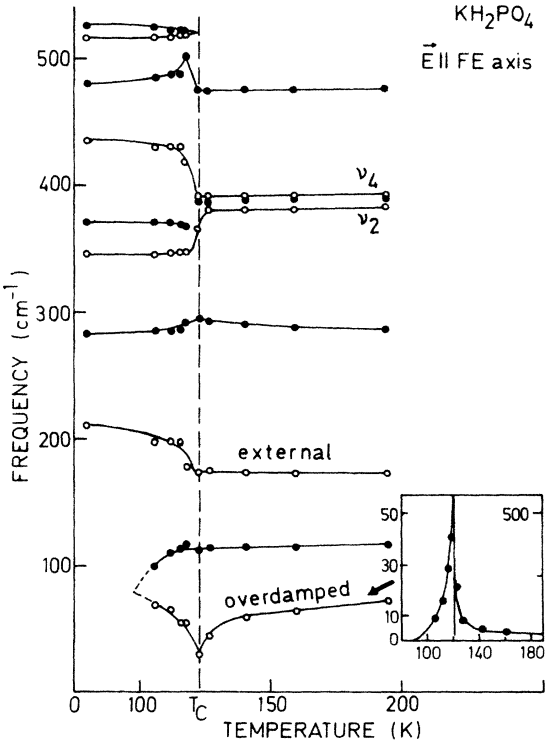

FIG. 7. Temperature dependence of the LO (full circles) and TO (open circles) lowest-frequency mode frequencies of KDP (polarization along the ferroelectric axis). Insert shows the temperature dependence of the oscillator strength of the overdamped soft mode. The lines are guides to the eye.

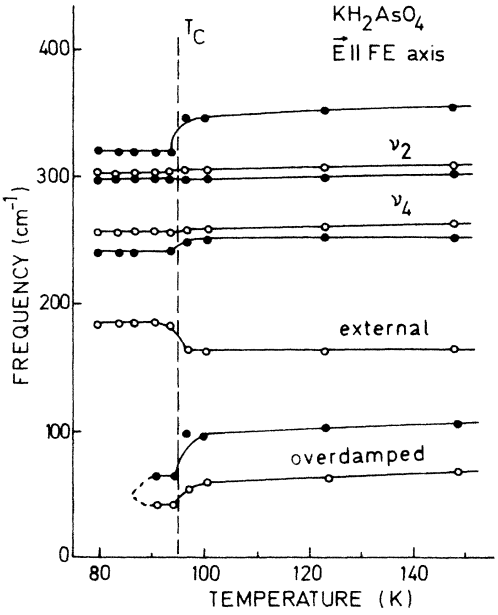

FIG. 8. Temperature dependence of the LO (full circles) and TO (open circles) lowest-frequency mode frequencies of KDA (polarization along the ferroelectric axis). The lines are guides to the eye.

tassium compounds, while it is continuous in the rubidium salt. This is consistent with the abrupt changes of frequencies within a narrower temperature range. (ii) The gap between the external translational mode and the ν_2-ν_4 group is smaller, and in terms of internal or external modes, the assignment should be regarded with precaution.

In KDA (Fig. 8), the oscillator strength of the 260 cm^{-1} mode is one order of magnitude larger than that of the 305 cm^{-1} mode. The oscillator strength of a ν_2 mode, infrared inactive for a regular tetrahedron, is expected to be smaller than that of a ν_4 mode. In the relevant scattering geometry $[x(yx)y]$ and in this spectral range, Raman spectra exhibit only one line[42] near 390 cm^{-1} in phosphate compounds and near 300 cm^{-1} in arsenate compounds. This Raman-active mode is very intense and therefore much more compatible with ν_2 assignment than ν_4, the latter usually being weakly Raman active. So the infrared modes lying at these frequencies are assigned to ν_2-like modes. Assignments in terms of internal (ν_2 or ν_4) and external modes in that case however should be regarded with some caution because their positions are close. Some transfer of mode parameters (eigenvector, oscillator strength, damping) has already occurred. In KDA, the ν_{4c} frequency does not shift down, because it is blocked between the LO external and the TO ν_2 modes. Frequency lowering of the external mode and the appearance of the overdamped soft mode are observed, and they may be considered consequences of the ν_{4c}-mode–proton-motion interaction.

It is now of interest to consider deuterated crystals. Infrared reflectivity experiments in DKDP samples are generally only somewhat conclusive because of surface-rehydrogenation problems.[24] However, Kawamura *et al.*[25] reported successfully the low-frequency spectra below 600 cm^{-1}. They observed that in the low-temperature phase, contrary to the hydrogenated compounds, the ν_{4c} mode is but slightly damped, while there is no large overdamped mode in the far infrared below 100 cm^{-1}. The high dielectric constant value originates in this case from polar excitations below the infrared range. Tunneling is known generally not to occur in deuterated crystals. Protons are known to tunnel at frequencies at least one order of magnitude larger than relaxational motions of deuterons. As a result, tunnel proton motions are expected to couple much more efficiently with lattice modes, compared to relaxations of deuterons. Results discussed above show that this is just what is observed experimentally. In hydrogenated compounds, tunneling thus seems to play a major role via strong coupling with the ν_{4c} mode, whereas no similar effect is observed in the deuterated compound. The ν_{4c}-mode softening is not properly necessary for the phase transition to occur. However, in the hydrogenated compounds, in particular in RDP, this mode appears to play an important role in coupling the protons to PO_4 distortion that ultimately leads to ferroelectricity.

B. *E* perpendicular to the ferroelectric axis

In this polarization, spectra must be strongly influenced by the proton intersite motions since the

latter vibrate in the plane perpendicular to the ferroelectric axis. Figure 9 shows the imaginary dielectric function at 80 K of the three compounds. Complete results of these simulations are reported elsewhere.[35] Like in the other polarization, comparison of the three compounds allows the assignment of the observed modes: (i) O—H bending modes at 1035 and 1300 cm^{-1}; (ii) ν_3 internal mode region, between 700 and 1300 cm^{-1}; (iii) ν_4-mode region, near 500 cm^{-1} in phosphates, 360 cm^{-1} in arsenate; (iv) translation and libration external modes at low frequencies.

No mode is seen at 3600 cm^{-1}, i.e., the natural frequency of O—H stretching vibrations. Therefore, one is forced to assign to proton stretching modes the bands observed at much lower frequency (1500–2500 cm^{-1}) and which are strongly damped. Figure 10 displays the temperature dependence of the imaginary dielectric function of RDP. Except for the measurement at 80 K, the TO response is characterized by a very broad excitation, the maximum of which lies at low frequency, but extends up to high frequencies in the O-H region, to such a degree that the imaginary dielectric function is nowhere negligible below 2000 cm^{-1}. This broad excitation is not an additional mode which would appear when approaching T_C from below, because no extra mode was added to those used to simulate the spectrum at 80 K. It is a contribution from all modes, originating in the high-frequency region: upon heating, progressively, modes interact and transfer their oscillator strengths and dampings from high- to low-frequency modes. The lowest-frequency mode is thus strongly enhanced in the vicinity of T_C. The dielectric constant anomaly observed in this direction is mainly due to the temperature dependence of this lowest-frequency coupled mode.

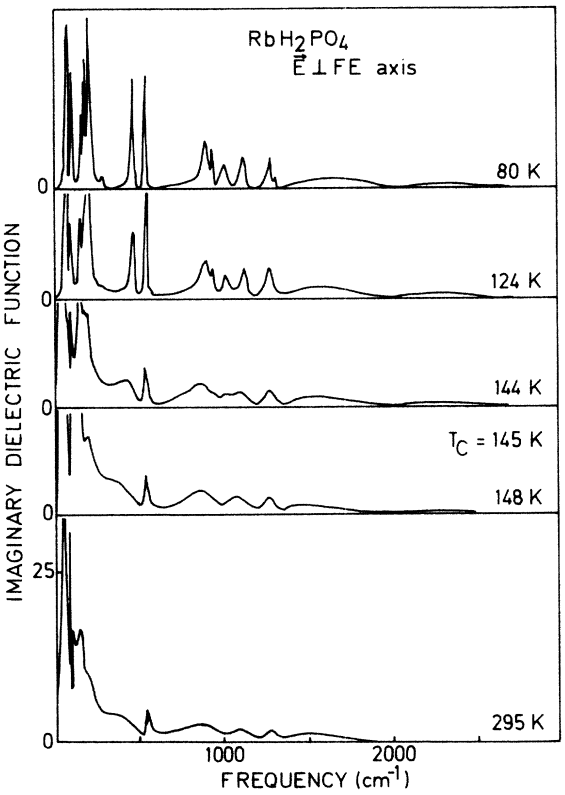

FIG. 10. Temperature dependence of the structure of the TO modes of RDP, for the polarization perpendicular to the ferroelectric axis (obtained by simulation with the four-parameter model).

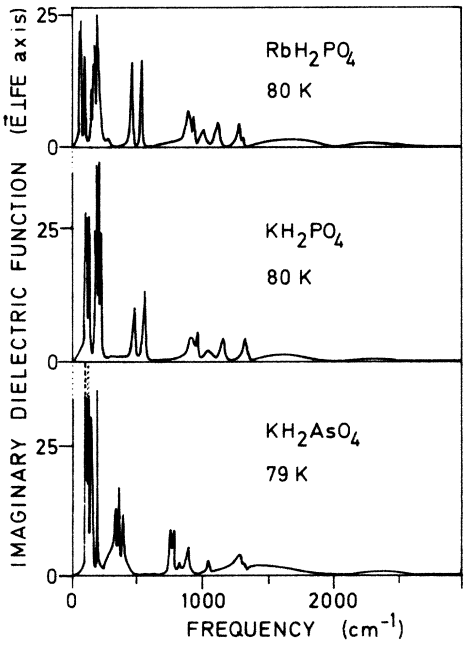

FIG. 9. Structure of the TO modes for the polarization perpendicular to the ferroelectric axis, for RDP (obtained by simulation with the four-parameter model), KDP and KDA (obtained by Kramers-Kronig inversion).

Details of the low-frequency region are displayed in Fig. 11, just above T_C. The five symmetry-predicted external modes are observed (see Table I), as well as both ν_4 internal modes. None of these modes is overdamped, and all exist at 80 K. Our results contrast with those recently reported by Wyncke and Bréhat[30] in KDP. They need an additional overdamped mode, which would only be present above or near T_C, to simulate their spectra with the four-parameter model. But their experimental spectral range is limited to frequencies below 400 cm^{-1}, and they introduce the higher-frequency contribution by a temperature-independent effective value of $\epsilon_\infty = 5.1$, whereas this contribution depends on temperature. They are then forced to introduce an additional overdamped mode to describe the spectra. The difficulties they encounter demonstrate the need to treat the entire coupled-mode systems 20–2500 cm^{-1}, since the imaginary dielectric function does not vanish over this spectral range.

C. Stabilization of the soft mode in the paraelectric phase

The sum of the TO-mode oscillator strengths is the lattice-mode contribution to the dielectric constant:

$$\epsilon_0 = \epsilon_\infty + \sum_j \Delta\epsilon_j \ . \tag{4}$$

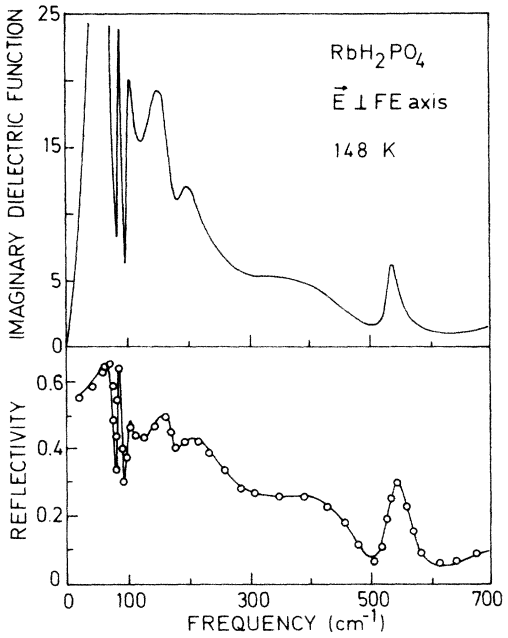

FIG. 11. Details of the low-frequency range of the TO-mode structure of RDP at $T_C + 3$ K (polarization perpendicular to the ferroelectric axis). Lower part: experimental infrared reflectivity spectrum (open circles) and best fit with the four-parameter model of the dielectric function (full line). Upper part: Structure of the TO polar modes, deduced from the simulation.

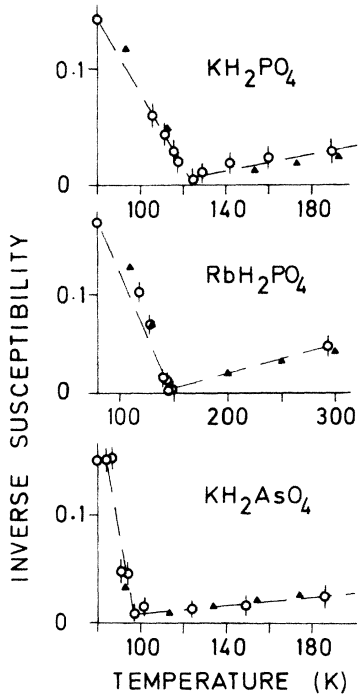

FIG. 12. Temperature dependence of the inverse dielectric constant. Open circles: values deduced from the TO-mode oscillator strengths via Eq. (4) for KDP, RDP, and KDA (polarization along the ferroelectric axis). Triangles: measurements in the microwave range, at 0.3 cm^{-1} for KDP (Ref. 41) and KDA, (Ref. 43) and at 5.1 cm^{-1} for RDP (Ref. 38). Dashed straight lines show Curie-Weiss behaviors.

The inverse dielectric constant calculated by Eqs. (3) and (4) is plotted versus temperature in Fig. 12, for the three compounds. Our values are consistent with measurements in the microwave range.[38,41,43] The experimental data lie almost on straight lines in both phases, according to the Curie-Weiss law. However, whereas the simplest Landau model predicts a ratio of slopes between the ferroelectric and paraelectric phase equal to 2, Fig. 12 shows much larger ratios. Similar temperature dependences of the susceptibility were reported by Raman scattering.[44] The high dielectric-constant level in the paraelectric phase is due to the oscillator strength of the enormous overdamped soft mode, the frequency of which increases only very slowly upon heating above the Curie temperature. This originates from the proton intersite motion, whose interaction with mode ν_{4c} persists to yield the soft mode: proton motions prevent the soft mode from rapid "hardening." It is suggested that the stabilization of the soft mode occurs via quartic anharmonicity, such as the nonlinear polarizability of heavy ions.[45]

D. Comparison with other techniques

KDP-type crystals have been investigated more extensively by Raman scattering than by infrared reflectivity. It is thus interesting to compare results obtained by both methods, and, for instance, our spectra of KDP (above T_C,B_2 symmetry) with the Raman data for TO (Ref. 32) and LO (Ref. 17) modes. Whereas Raman spectra clearly exhibit the TO and LO components of the ferroelectric soft mode, the TO heavy-ion external mode is very weak, and its LO counterpart invisible. The nonobservation of LO lines prevents the calculation of dielectric strengths. Conversely, it must be kept in mind that in infrared reflectivity, the intensities of the modes are their dielectric strengths, viz., the essential physical quantity for ferroelectrics, whereas there is no such direct relation with Raman line intensities. The ν_2 mode (TO and LO) gives rise to sharp intense diffusion, while ν_3 and ν_4 lines are very broad, and split into two components. The frequencies of ν_2 and external modes are identical within experimental error when obtained by both techniques, but there is a large discrepancy for the ν_{4c} mode (about 475 cm^{-1} for the maximum of the Raman broad line, 400 cm^{-1} for the modulus of the complex pole deduced from infrared spectra). Such a difference may be explained as follows: there are two interacting modes, one sharp (ν_2) and the other strongly damped (ν_4). The ratio of intensities of both modes is different between Raman and infrared, and the value of this ratio is responsible for the spectral shape in this case of discrete state-continuum Fano-like interference, so the resulting profiles may be rather different in infrared reflectivity and Raman scattering. Figure 13 illustrates this schematically: the full line is the B_2 (TO) Raman spectrum reported by Coignac and Poulet,[32] with the strong narrow ν_2 mode lying just below 400 cm^{-1} and another

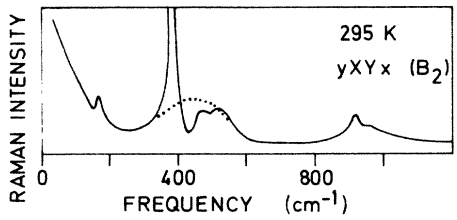

FIG. 13. Raman spectrum (full line) obtained by Coignac and Poulet (Ref. 32) in KDP. The dotted line shows schematically the scattering line profile that could be expected for mode ν_{4c} if mode ν_2 (responsible for the strong narrow line just below 400 cm^{-1}) were inactive.

broad maximum around 500 cm^{-1}. The maximum of the ν_{4c} line would be strongly shifted by Fano interference with respect to its position if both modes did not interfere as shown schematically in Fig. 13 by a dotted line.

As reviewed in the Introduction, a new interpretation of the mechanism of the phase transition, which would be of order-disorder type, was recently formulated. This interpretation is based upon the observation in the paraelectric phase of Raman lines which are symmetry forbidden, whereas they are allowed in the ferroelectric phase. These lines correspond to modes ν_1, ν_3, ν_4, and to the tetrahedron libration mode. But none of these modes is forbidden by the symmetry of the paraelectric phase, but only by the scattering geometry: each of them is allowed in at least one other scattering geometry. The appearance of these "forbidden" modes might be related to depolarizing or nonlinear effects related to the lack of inversion symmetry of the crystals. For example, the reflection of the laser beam upon the back crystal surface may generate modes with mixed TO-LO character. Moreover, one may speculate that the existence of an overdamped mode implies that there are very slow, quasistatic fluctuations, which can locally distort the lattice and activate symmetry-forbidden

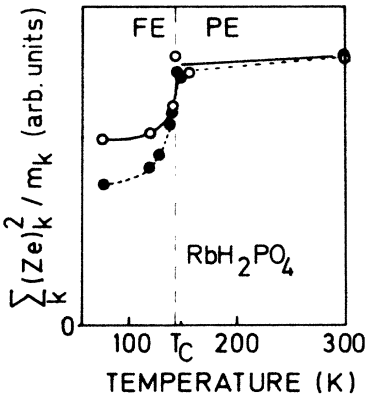

FIG. 14. Temperature dependence of the sum of the squared effective charges of the ions weighted by their masses [obtained by Eq. (5)] for RDP, in the direction of the ferroelectric axis (full circles) or perpendicular to it (open circles). The lines are guides to the eye.

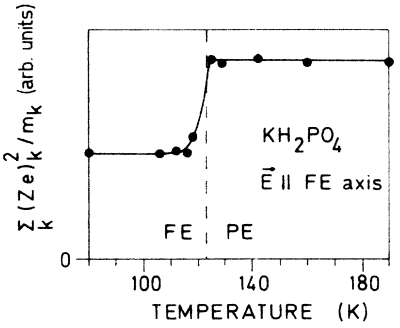

FIG. 15. Temperature dependence of the sum of the squared effective charges of the ions weighted by their masses [obtained by Eq. (5)] for KDP, in the direction of the ferroelectric axis. The line is a guide to the eye.

modes at Raman time scales. It must be emphasized that by infrared reflectivity, all symmetry-forbidden modes unambiguously disappear at T_C. In true order-disorder systems, such as $NaNO_2$ or NH_4AlF_4, symmetry forbidden modes are clearly observed several 10 K above T_C in infrared reflectivity[46] or in Raman spectra.[47] This is even an additional argument in favor of the displacive character of the phase transition of KDP and related compounds. Our results agree with the high-resolution neutron-diffraction experiments by Nelmes *et al.*,[3] who showed the thermal agitation factors of the heavy ions to be phononlike, while the proton ones are order-disorder-like. This is also consistent with the recent nuclear quadrupolar resonance work by Blinc,[48] from which all oxygens are equivalent in the whole paraelectric phase at the NQR time scale. All these results seem very difficult to interpret in terms of the heavy-ion order-disorder model reviewed in Ref. 13.

V. EFFECTIVE CHARGES

Knowledge of the *entire* set of TO- and LO-mode frequencies, given by the four-parameter simulation, allows us to evaluate the effective charges of the different ions[22,49]

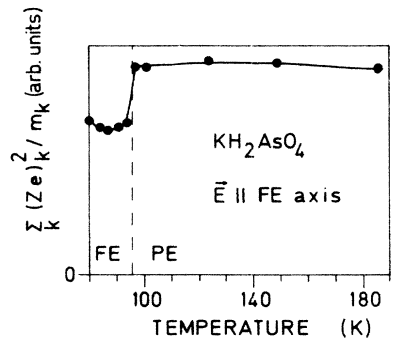

FIG. 16. Temperature dependence of the sum of the squared effective charges of the ions weighted by their masses [obtained by Eq. (5)] for KDA, in the direction of the ferroelectric axis. The line is a guide to the eye.

$$\sum_j (\Omega_{jLO}^2 - \Omega_{jTO}^2)_\alpha = \frac{1}{\epsilon_V V} \sum_k \frac{(Ze)_{k\alpha}^2}{m_k} \quad (5)$$

where ϵ_V denotes the dielectric constant of vacuum, $(Ze)_{k\alpha}$ is the effective charge of atom k in direction α (the polarization) contained in volume V, and m_k is its mass. The concept of effective charges is useful to characterize the variation of the chemical bonds with temperature. Electrical neutrality provides another relation

$$\sum_k (Ze)_{k\alpha} = 0 \; . \quad (6)$$

In the case of two nonequivalent ions, these equations can be solved for the $(Ze)_{k\alpha}$'s. For KDP-type crystals, which contain four nonequivalent ions in the paraelectric phase, the system remains undetermined. It is only possible to calculate the sum of the squared effective charges of the ions, weighted by their masses. The left-hand side of Eq. (5) is plotted versus temperature in Fig. 14, for RDP, for both polarizations. The effective charges decrease strongly just below T_C. This decrease is consistent with the shortening of the cation-anion bond lengths that occurs at the phase transition, and which is responsible for the appearance of the spontaneous polarization, and constitutes the signature of ferroelectricity.[22,49,50] The decrease is less marked perpendicularly to the ferroelectric axis than along it, as it should be. Figures 15 and 16 exhibit similar behavior for KDP and KDA along the ferroelectric axis. These features are consistent with a displacive character of the phase transition.

ACKNOWLEDGMENTS

We are indebted to D. Rytz and G. Hauret for supplying the samples of KDP and RDP. Fruitful discussions with G. Hauret and M. Vallade are also gratefully acknowledged.

[1]G. Busch and P. Scherrer, Naturwissenschaften **23**, 737 (1935).
[2]R. J. Nelmes, Ferroelectrics **53**, 207 (1984).
[3]R. J. Nelmes, W. F. Kuhs, J. E. Howard, J. E. Tibballs, and T. W. Ryan, J. Phys. C **18**, L1023 (1985).
[4]R. Blinc, J. Phys. Chem. Solids **13**, 204 (1960).
[5]P. G. De Gennes, Solid State Commun. **1**, 132 (1963).
[6]K. Kobayashi, J. Phys. Soc. Jpn. **24**, 497 (1968).
[7]A. S. Barker and M. Tinkham, J. Chem. Phys. **38**, 2257 (1963).
[8]I. P. Kaminow and T. C. Damen, Phys. Rev. Lett. **20**, 1105 (1968).
[9]P. S. Peercy, Phys. Rev. Lett. **31**, 379 (1973).
[10]R. Blinc and B. Zeks, *Soft Modes in Ferroelectrics and Antiferroelectrics* (North-Holland, Amsterdam, 1974).
[11]M. E. Lines and A. M. Glass, *Principles and Applications of Ferroelectrics and Related Materials* (Clarendon, Oxford, 1977).
[12]R. Blinc, B. Zeks, and R. J. Nelmes, Phase Transitions **3**, 293 (1983).
[13]M. Tokunaga and I. Tatsuzaki, Phase Transitions **4**, 97 (1984).
[14]T. Matsubara, Jpn. J. Appl. Phys. Suppl. **24-2**, 1 (1985).
[15]H. Z. Cummins, Philos. Trans. R. Soc. London, Ser. A **293**, 393 (1979).
[16]M. Tokunaga, Y. Tominaga, and I. Tatsuzaki, Ferroelectrics **63**, 171 (1985).
[17]Y. Tominaga, M. Kasahara, H. Urabe, and I. Tatsuzaki, Solid State Commun. **47**, 835 (1983).
[18]Y. Tominaga, H. Urabe, and M. Tokunaga, Solid State Commun. **48**, 265 (1983).
[19]Y. Tominaga, M. Tokunaga, and I. Tatsuzaki, Solid State Commun. **54**, 979 (1985).
[20]H. Tanaka, M. Tokunaga, and I. Tatsuzaki, Solid State Commun. **49**, 153 (1984).
[21]J. L. Martinez, J. M. Calleja, and J. A. Gonzalo, Solid State Commun. **52**, 1 (1984).
[22]F. Gervais, in *Infrared and Millimeter Waves*, edited by K. J. Button (Academic, New York, 1983), Vol. 8, Chap. 7, p. 279.
[23]F. Sugawara and T. Nakamura, J. Phys. Soc. Jpn. **28**, 158 (1970).
[24]S. Levin, I. Pelah, and E. Wiener-Avnear, Phys. Status Solidi B **58**, 61 (1973).
[25]T. Kawamura, A. Mitsuishi, N. Furuya, and O. Shimomura, Opt. Commun. **10**, 337 (1974).
[26]A. S. Barker and J. J. Hopfield, Phys. Rev. **135**, A1732, (1964).
[27]K. E. Gauss, H. Happ and G. Rother, Phys. Status Solidi B **72**, 623 (1975).
[28]D. A. Ledsham, W. G. Chambers, and T. J. Parker, Infrared Phys. **17**, 165 (1977).
[29]F. Bréhat and B. Wyncke, Phys. Status Solidi B **128**, 83 (1985).
[30]B. Wyncke and F. Bréhat, J. Phys. C **19**, 2649 (1986).
[31]T. Kurosawa, J. Phys. Soc. Jpn. **16**, 1298 (1961).
[32]J. P. Coignac and H. Poulet, J. Phys. (Paris) **32**, 679 (1971).
[33]U. Fano, Nuovo Cimento **12**, 156 (1935); Phys. Rev. **124**, 1866 (1961).
[34]G. Breit and E. Wigner, Phys. Rev. **49**, 519 (1936).
[35]P. Simon, Thèse de Doctorat, Université d'Orléans, 1986.
[36]V. C. Farmer, *The Infrared Spectra of Minerals* (The Mineralogical Society, London, 1974).
[37]M. El Sherif, F. Bréhat, B. Wyncke, and A. Hadni, Int. J. Infrared Millim. Waves **5**, 815 (1984).
[38]A. A. Volkov, G. V. Kozlov, and S. P. Lebedev, Kratkie Soobshcheniya po Fisike **9**, 37 (1979) [Sov. Phys.—Lebedev Institute Reports **9**, 35 (1979)].
[39]M. Chabin and F. Gilletta, Ferroelectrics **15**, 149 (1979).
[40]A. A. Volkov, G. V. Kozlov, and S. P. Lebedev, Fiz. Tverd. Tela (Leningrad) **20**, 2021 (1978) [Sov. Phys.—Solid State **20**, 1166 (1978)].
[41]I. P. Kaminow and G. O. Harding, Phys. Rev. **129**, 1562 (1963).
[42]M. A. Scarparo, R. S. Katiyar, R. Srivastava, and S. P. S. Porto, Phys. Status Solidi B **90**, 543 (1978).
[43]I. P. Kaminow, Phys. Rev. **138**, A1539 (1965).
[44]C. M. Wilson and H. Z. Cummins, in *Proceedings of the Second International Conference on Light Scattering in Solids*, edited by M. Balkanski (Flammarion, Paris, 1971), p. 420.

[45]A. Bussman-Holder and H. Bilz, Ferroelectrics **54**, 5 (1984); and in *Proceedings of the Second International Conference on Phonon Physics,* edited by J. Kollar, N. Kroo, N. Menyhard, and T. Siklos (World-Scientific, Singapore, 1985), p. 299.
[46]F. Bréhat and B. Wyncke, J. Phys. C **18**, 1705 (1985).
[47]M. Couzi, P. Rocquet, and J. L. Fourquet, J. Phys. (Paris) **46**, 435 (1985).
[48]R. Blinc, Z. Naturforsch. A **41**, 249 (1986).
[49]F. Gervais and H. Arend, Z. Phys. B **50**, 17 (1983).
[50]F. Gervais, P. Simon, P. Echegut, and B. Calès, Jpn. J. Appl. Phys. Suppl. **24-2**, 117 (1985).